ACS APPLIED MATERIALS & INTERFACES

Research Article

www.acsami.org

Conformal Atomic Layer Deposition of Alumina on Millimeter Tall, Vertically-Aligned Carbon Nanotube Arrays

Kelly L. Stano,[†] Murphy Carroll,[†] Richard Padbury,[†] Marian McCord,[†,‡,§] Jesse S. Jur,[†] and Philip D. Bradford*[,†]

[†]Department of Textile Engineering, Chemistry and Science, North Carolina State University, Raleigh, North Carolina 27695-8301, United States

[‡]Joint Department of Biomedical Engineering, North Carolina State University, Raleigh, North Carolina 27695-7115, United States

[§]University of North Carolina, Chapel Hill, North Carolina 27599, United States

Supporting Information

ABSTRACT: Atomic layer deposition (ALD) can be used to coat high aspect ratio and high surface area substrates with conformal and precisely controlled thin films. Vertically aligned arrays of multiwalled carbon nanotubes (MWCNTs) with lengths up to 1.5 mm were conformally coated with alumina from base to tip. The nucleation and growth behaviors of Al_2O_3 ALD precursors on the MWCNTs were studied as a function of CNT surface chemistry. CNT surfaces were modified through a series of post-treatments including pyrolytic carbon deposition, high temperature thermal annealing, and oxygen plasma functionalization. Conformal coatings were achieved where post-treatments resulted in increased defect density as well as the extent of functionalization, as characterized by X-ray photoelectron spectroscopy and Raman spectroscopy. Using thermogravimetric analysis, it was determined that MWCNTs treated with pyrolytic carbon and plasma functionalization prior to ALD coating were more stable to thermal oxidation than pristine ALD coated samples. Functionalized and ALD coated arrays had a compressive modulus more than two times higher than a pristine array coated for the same number of cycles. Cross-sectional energy dispersive X-ray spectroscopy confirmed that Al_2O_3 could be uniformly deposited through the entire thickness of the vertically aligned MWCNT array by manipulating sample orientation and mounting techniques. Following the ALD coating, the MWCNT arrays demonstrated hydrophilic wetting behavior and also exhibited foam-like recovery following compressive strain.

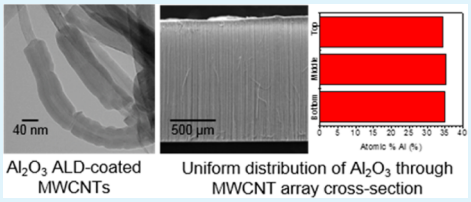

Al_2O_3 ALD-coated MWCNTs

Uniform distribution of Al_2O_3 through MWCNT array cross-section

KEYWORDS: *carbon nanotube (CNT), atomic layer deposition (ALD), alumina, aligned carbon nanotube array, CNT−inorganic hybrid, plasma, functionalization*

1. INTRODUCTION

Carbon nanotube (CNT)−inorganic hybrids are a class of functional materials which have drawn widespread and increasing interest in recent years.[1] As opposed to nanocomposites where the CNT and inorganic phases are combined via mechanical means, CNT−inorganic hybrids are characterized by CNTs which are coaxially coated with thin layers of inorganic material. Due to interfacial charge transfer processes and size domain effects, the CNT−inorganic hybrids are expected to exhibit a synergistic set of enhanced physical properties. CNTs are an interesting template for these hybrids as they possess superior mechanical, thermal, and electrical properties, while simultaneously being low density and of high surface area. There is considerable difficulty, however, in achieving smooth, conformal, and pinhole free coatings on CNTs for three major reasons: (1) the inherent chemical inertness of high crystallinity and purity CNTs, (2) the tendency of CNTs to bundle and agglomerate due to large van der Waals forces, and (3) the lack of synthesis methods suitable for coating 3D and aligned CNT architectures.

Atomic layer deposition (ALD) is a versatile technique used to conformally deposit a wide variety of multifunctional materials onto complex micro- and nanosized structures with atomic scale precision. Using ALD, a variety of metal oxides and metals have been deposited on CNTs including Al_2O_3,[2] HfO_2,[3] ZrO_2,[4] TiO_2,[5] SiO_2,[5] ZnO,[6,7] V_2O_5,[8] Pt,[9,10] Ru,[11] and W[12] for a wide range of applications including catalysis,[9,10] Li-ion batteries,[13] field-effect transistors,[14] and many others.[11] The trimethylaluminum and water ALD process used to form Al_2O_3 nanoscale coatings has a favorable Gibbs free energy of formation between the reactants and products which allows for "ideal" ALD growth behavior in a relatively wide temperature range from 30 to 300 °C.[15−18] Al_2O_3 is an attractive material to coat CNTs due to its excellent thermal stability and resistance to corrosion.

Several studies have demonstrated the ability to successfully coat multiwalled CNTs (MWCNTs) with Al_2O_3 via ALD

Received: August 1, 2014
Accepted: October 2, 2014
Published: October 2, 2014

without any post-treatment to activate the MWCNT surfaces.[2,6,12,13] In these instances, the defect density in the MWCNT walls is high enough that they act as nucleation sites for deposition and growth. For many applications, however, MWCNTs with large amounts of defects are highly undesirable as they degrade the MWCNTs' physical properties. Much like single-walled CNTs (SWCNTs), MWCNTs of high purity and low defect density will not readily nucleate the growth of conformal thin films due to their surfaces being nonreactive and chemically inert toward the ALD precursors.[19−21] This leads to sparse nucleation and the development of a bead-like structure on the CNT surface instead of a uniform coating.[3] This has been overcome through the development and application of covalent and noncovalent functionalization techniques which promote interaction between the CNT surface and precursor.

To promote conformal ALD coating, a common method of covalent functionalization of MWCNT surfaces is via refluxing in concentrated sulfuric and nitric acids.[22] This results in the creation of carboxyl and hydroxyl groups on the MWCNT surfaces, which act as surface reaction sites for ALD precursors corresponding to conformal ALD growth.[5,8,23] However, this method is aggressive and creates many defects on the MWCNT walls which degrades their physical properties. Additionally, this method is not suitable for the functionalization of aligned MWCNT arrays as wet-processing will disrupt the MWCNT alignment and cause bundling and agglomeration upon drying. Alternatively, gas-phase covalent functionalization via oxygen plasma treatment has been used on aligned MWCNT arrays as well as MWCNT powders to promote the ALD nucleation of Pt.[9,10] Though effective, covalent modification of MWCNTs and SWCNTs alters their intrinsic optical, electrical, and mechanical properties. For this reason, noncovalent functionalization techniques have been explored as a method of weakly bonding the CNT surface to the ALD film via an adhesion layer. Farmer and Gordon accomplished this by adsorbing NO_2 molecules to the surfaces of suspended SWCNTs, and then reacting TMA with the adsorbed NO_2 to yield a stable and uniform seed layer for subsequent coating with Al_2O_3.[24] Using this same method, Cavanagh et al. conducted ALD on gram quantities of MWCNTs, but it was shown that the deposited Al_2O_3 coating was free to slide along MWCNTs due to the lack of covalent bonding between adjacent layers.[25]

Despite the intense interest in his field, the application of ALD thin film techniques to 3D CNT architectures such as vertically aligned CNT arrays (VACNTs) has not been fully explored. Not only do arrays present a unique set of issues for functionalization, but due to their ultrahigh aspect ratios and surface area, special considerations must be made regarding the ALD processing parameters. Adequate dosing and purging time must be provided for the full diffusion of precursor into and out of the array structure in order to ensure ideal ALD-type growth. Additionally, high aspect ratio structures are prone to nonuniformly distributed coatings due to gas flow effects in the reactor and within the sample.[26−28] It is important to mitigate these effects so that property enhancement may be achieved via conformal coating along the entire length of the CNT rather that preferential accumulation at the top of the array.

In this work, we present a systematic study of various gas-phase MWCNT surface modifications and their associated effects on the nucleation and growth of Al_2O_3 ALD coatings on high graphitic quality, low defect density VACNT arrays. Once the MWCNT surfaces were optimized to achieve conformal ALD coatings, sample orientation and mounting techniques were explored in order to promote full precursor infiltration and purging. As a result, 1.5 mm tall VACNT arrays were uniformly and conformally ALD coated with Al_2O_3 from base to tip without increasing precursor exposure time.

2. MATERIALS AND METHODS

2.1. Aligned MWCNT Growth. VACNT arrays were grown on quartz substrates via chlorine mediated low-pressure chemical vapor deposition (CVD) using iron(II) chloride, anhydrous (99.5%, VWR) catalyst, and acetylene carbon precursor.[29] After 20 min of growth, the resulting arrays were 1.5 mm tall with an average MWCNT diameter of 43 nm, as measured from TEM images. While the MWCNT aspect ratio is ∼35 000, the pore aspect ratio is ∼15 000 corresponding to a MWCNT spacing of approximately 100 nm.

2.2. MWCNT Surface Modification. Three treatments were used to modify the as-grown VACNT surface chemistry, graphitic quality, and defect density. These included CVD of pyrolytic carbon (PyC), high-temperature graphitization (G), and O_2/CF_4 plasma functionalization (O_2). For PyC treatment, the VACNTs were conformally coated with PyC using CVD. Samples were heated in a vacuum in a quartz tube furnace. At 800 °C, C_2H_2 began to flow at 600 sccm, and the pressure of the system was maintained at 30 Torr. After 5 min, C_2H_2 flow was stopped, and the system was cooled while being purged with Ar gas.

The O_2/CF_4 plasma treatment was conducted in a capacitively coupled dielectric barrier discharge atmospheric pressure plasma system. The custom-built system consists of two parallel Cu plate electrodes (60 × 60 cm^2), with a spacing of 3 cm. The plasma was operated by a 4.8 kW audio frequency power supply at 1.67 kHz. All treatments were carried out for 5 min in 1.0% oxygen + 1.0% CF_4 + 98% helium gas mixture (by mass).

Finally, the graphitization treatment (G) was carried out in a Red Devil Webb 124 high-temperature graphite furnace (R. D. Webb Company, Natick MA, USA). After removing the VACNT from the quartz substrate and loading it into the furnace, the chamber was evacuated with a vacuum pump. The sample was heated from 25 to 1500 °C at a rate of 25 °C per minute and then soaked at 1500 °C for 25 min. Following the dwell stage, the sample was heated from 1500 to 2000 °C at a rate of 15 °C per minute. During this step, at 1750 °C, the chamber was refilled with argon and kept there under a continuous flow of argon at 7.5 scfh. After dwelling at 2000 °C for 15 min, the temperature ramped up to 2150 °C at a rate of 3 °C per minute. Upon reaching 2150 °C, the program terminated and the furnace was left to cool, switching the chamber back to vacuum at ∼1750 °C.

The three post-treatments were used alone and in combination on the VACNT arrays to make five of the six distinct samples for these experiments: PyC, G, O_2, PyC+O_2, and G+O_2. An as-grown sample was used as a control throughout the study and is referred to as "Pristine."

2.3. ALD of Al_2O_3. Al_2O_3 ALD was performed in a custom hot wall viscous flow reactor at 100 °C and 1 Torr using trimethylaluminum (TMA, 98% Strem Chemicals, Inc.) and biotechnology performance certified grade high purity water (Sigma-Aldrich) as a precursor and coreactant, respectively. The pressure of the viscous flow reactor was kept constant at 1 Torr via an Alcatel 2021SD mechanical pump and an MKS (model PR4000B) flow controller with a nitrogen gas flow rate of approximately 400 sccm. The ALD process began with an N_2 purge of 300 s followed by an ALD cycle sequence of TMA/N_2/H_2O/N_2 = 0.2:30:0.2:45 s, which was repeated for the desired number of cycles. Separate experiments were carried out with the arrays oriented parallel and perpendicular to the flow of gas through the reactor. The MWCNT arrays were attached to the front of the sample stage via loops of thermally stable Kapton tape between the quartz substrate and the sample stage (for parallel orientation to the gas flow) or an angle bracket that was screwed into the front of the stage (for perpendicular orientation to the gas flow) and were then moved to the center of the ALD reactor. Photographs depicting sample mounting techniques are provided in the Supporting Information (S1).

For the majority of experiments in this study, the VACNT arrays were coated with 100 cycles of alumina ALD. They are labeled as such: VACNT_100, PyC_100, G_100, O_2_100, PyC+O_2_100, and G +O_2_100. For compression testing, TGA samples were coated with 500 cycles of Al_2O_3 ALD and are labeled accordingly.

2.4. Characterization. Scanning electron microscopy (SEM) was conducted on a JEOL JSM-6400F field-emission SEM with a beam voltage of 10 kV and a Hitachi S3200 variable-pressure SEM fitted with a 4Pi Isis energy dispersive spectrometer (EDS) system. Elemental spectra were gathered over an acquisition time of 100 s, and accompanying images were taken with a beam voltage of 20 kV. For quantitative elemental analysis, the collected spectra were compared to an Al_2O_3 standard. Transmission electron microscopy (TEM) images were taken using a Hitachi HF2000 cold field emission TEM with a beam voltage of 200 kV. A probe sonicator was used to disperse 0.001 g of CNTs in 10 mL of ethanol. The mixture was pulse sonicated (1 s on, 0.3 s off) in an ice bath for 1 h. Immediately following ultrasonication, a small amount of the dispersion was deposited on holey carbon mesh and Cu TEM grids and then allowed to dry. The graphitic quality and defect density of the MWCNT arrays was analyzed using a Renishaw Ramascope with a laser wavelength of 514.5 nm focused to the sample using a using a Renishaw microscope with 50× objective. Five measurements were taken from different locations on each sample, and the collected data were averaged. Thermogravimetric analysis (TGA) experiments were conducted on a PerkinElmer Pyris 1 TGA using 5−10 mg of each sample heated at a rate of 10 °C/min in air to 900 °C, and then isothermally soaked for 30 min. The compressive properties of MWCNT-Al_2O_3 nanocomposites were measured using an Instron 5544 mechanical tester operated in compression mode. Platens were custom-designed and fabricated to fit securely in the clamp holders to prevent unwanted instrument compliance. The top platen measured 3.175 cm in diameter, while the bottom measured 5 cm, which allowed for total coverage of all arrays tested. The load rate was set to 0.1 mm/min, and a 2 kN load cell was used for all samples.

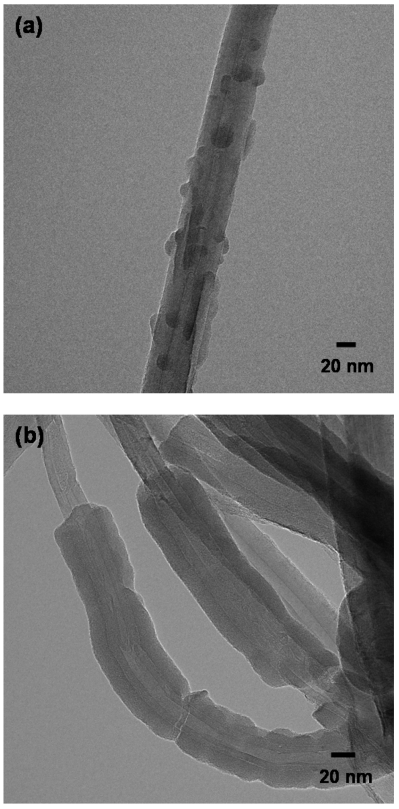

Figure 1. TEM micrographs taken after 100 cycles of Al_2O_3 ALD on (a) VACNT_100 and (b) PyC+O_2_100 (PyC deposited and plasma functionalized) MWCNTs.

3. RESULTS AND DISCUSSION

3.1. Conformal Coating of MWCNTs. An example VACNT array used in these experiments is shown in Figure S2. After 20 min of growth, the arrays measured 1.5 mm tall with individual MWCNTs having an average diameter of 43 nm. The calculated aspect ratio of these MWCNTs was ∼1:35 000, and the average specific surface area as measured by BET was 40 m^2/g. An EDS spectrum (Figure S3) taken from an as-grown array detected only 0.96 atom % and 0.42 atom % O and Fe, respectively, indicating rather high purity.

Al_2O_3 ALD on as-grown VACNT arrays resulted in the surface nucleation and growth of beads or nanospheres as depicted in Figure 1a. TEM micrographs taken after 25, 75, and 100 cycles are shown in Figure S4. After 25 cycles, only sparse nucleation can be seen on the MWCNT surface. Increasing the number of cycles resulted in the growth of the nucleated Al_2O_3, with some local coalescence. After 100 cycles, the MWCNT surface was covered with large, monodisperse Al_2O_3 beads. The Al_2O_3 morphology was indicative of substrate-inhibited island growth where a lack of −OH functional sites for TMA reaction results in poor nucleation.[30] Due to the lack of a conformal surface functionality, precursor molecules chemisorb at defect sites on the MWCNT surface and subsequently nucleate to grow disparate beads. This nonideal growth mode has been demonstrated predominantly on SWNTs,[3,19] which have comparatively fewer defects than MWCNTs. In fact, the majority of prior work in ALD coating of MWCNTs with Al_2O_3 has demonstrated facile and conformal coating on MWCNTs without any functionalization treatment.[2,6,12,13] Since the nucleation of Al_2O_3 relies on the presence of surface −OH groups and/or a high concentration of defects in the CNT walls, it is likely that the MWCNTs from previous studies had higher amounts of defects. Similar to the findings from Cavanagh et al., the MWCNTs grown and used for this study likely had a much lower defect density than those used in previous work, and thus did not readily nucleate and grow conformal Al_2O_3 films on unfunctionalized surfaces.[25]

Two additional control samples were synthesized in order to evaluate ALD coating uniformity on MWCNTs with a variety of graphitic qualities and amorphous contents. This was achieved via post-treatment of as-grown MWCNTs with high temperature graphitization and PyC deposition. TEM micrographs of samples G_100 and PyC_100 after 100 Al_2O_3 ALD cycles are shown in Figure S5. The Al_2O_3 morphology on graphitized MWCNTs appears similar to that seen on as-grown CNTs with coverage of monodisperse beads. During high temperature annealing of MWCNTs, amorphous and graphitic defects can be healed.[31,32] Long soak times at high temperature in an inert atmosphere allow disordered carbon atoms at defect sites to rearrange, thus increasing the degree of graphitization but also decreasing nucleation sites for Al_2O_3 growth.

The nucleation and growth behavior of ALD Al_2O_3 on PyC coated MWCNTs appeared different compared to the other controls. The particles were no longer monodisperse, instead having a wide range of diameters. Additionally, the deposited material formed both smooth, round beads as well as angular and plate-like morphologies. This can be attributed to the increased surface roughness created during PyC deposition. PyC formed via thermal decomposition of C_2H_2 is a mixture of sp^2−sp^3 hybridized carbon molecules. This technique has been used to radially grow MWCNTs, where additional walls are

deposited in a layer-by-layer fashion.[33,34] Characteristic of this mechanism, the roughness of the film increases as a partial layer is formed, only decreasing once the layer is complete. The areas of roughness resemble high surface energy MWCNT wall defects, and thus act as sites for nucleation. Jensen et al. demonstrated conformal Al_2O_3 coatings on MWCNT arrays using amorphous carbon pretreatment.[35] In our case, however, PyC deposition alone was not enough to achieve smooth films.

To enhance Al_2O_3 nucleation and coating uniformity, functionalization treatment was employed to modify the MWCNT surface chemistry and thus MWCNT-TMA reactivity. Pristine, PyC coated, and graphitized VACNT arrays were treated for 5 min in O_2/CF_4 plasma before being deposited with 100 cycles of Al_2O_3. All plasma treated samples exhibited a significant improvement in conformality of the Al_2O_3 coating compared to the nonfunctionalized controls. TEM images taken at low magnification (Figure S6a,c,e) show many Al_2O_3-coated MWCNTs, which was exemplary of the entire grid. The smoothest and most conformal Al_2O_3 coatings were formed for PyC+O_2_100, as shown in Figure 1b. The average deposition rate of Al_2O_3 on each sample was calculated to be within 1.0−1.3 Å/cycle, using measurements taken from high-magnification TEM micrographs. This deposition rate is typical for the ALD parameters used.[15−17]

Improvement in Al_2O_3 film quality is attributed to increased nucleation site density from surface activation. Defects are incurred to MWCNTs upon plasma treatment due to ion bombardment and breakage of sp^2 bonds. When treated in an oxidizing environment like O_2, defects and dangling bonds can be satisfied by an oxygenated species. Oxygen-containing functional groups react with TMA to nucleate Al_2O_3.[18] A higher concentration of reactive sites results in dense nucleation along the MWCNT surface. These nuclei quickly grow and coalesce due to favorable surface energy to form smooth films. O_2 plasma treatment has also been shown to be an effective means for improving the uniformity of Pt nanoparticle distribution on MWCNT surfaces deposited via ALD.[9] In the TEM micrographs, there are obvious areas where it appears that the Al_2O_3 film has cracked and slid along the length of the MWCNTs. This "macaroni on a string" morphology has been previously reported by Cavanagh et al.,[25] and it is suspected that ultrasonication caused the deposited film to break, slip, and even be completely removed in areas of the MWCNTs.

XPS spectra, shown in Figure 2, confirm the presence of oxygen-containing functional groups on PyC deposited and plasma treated arrays. Before any treatment, only the C 1s peak was visible (~285 eV), indicating that the concentrations of oxygen or other impurities are below the detection limit of the instrument. After 5 min of PyC deposition, the XPS spectrum remained unchanged. Following the 5 min O_2/CF_4 plasma treatment, O 1s and F 1s peaks became apparent in the survey scan, each comprising ~5 atom %. The high resolution O 1s scan for plasma treated MWCNTs is majorly symmetric and centered over 533 eV, corresponding to carbon atoms with single oxygen bonds (O−C).[36] Despite the presence of oxygen, however, high resolution spectra collected for arrays with and without plasma treatment show no change in the shape of the C 1s peak. This indicates that there is no significant change in the nature of carbon−carbon bonding on the MWCNT surface, whether in the form of defects, functional groups, or other sp^3 carbon species. This is reasonable due to the low concentrations of O_2 and CF_4 (1%) in He and the short duration of the plasma treatment (5 min). O_2/CF_4 plasmas are commonly

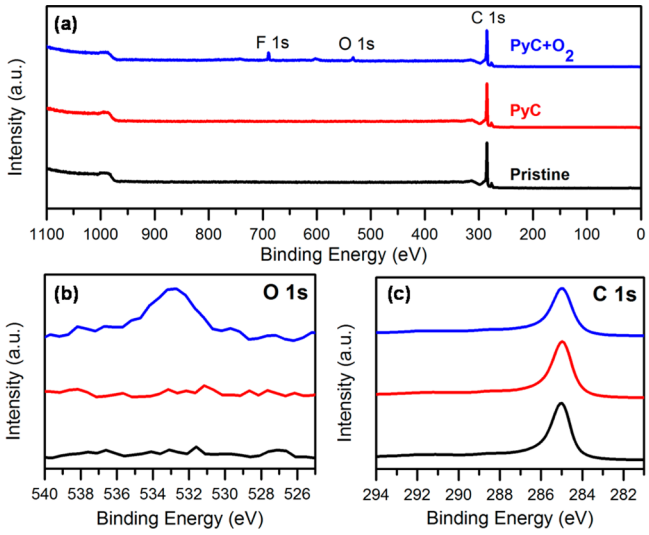

Figure 2. XPS spectra (a) survey and high resolution scans of the (b) O 1s and (c) C 1s collected for pristine, PyC deposited, and plasma treated MWCNT arrays. Only the C 1s peak is visible for nonplasma treated arrays, but O 1s and F 1s peaks are found in PyC+O_2.

used to modify the surface chemistry of polymer films to affect surface energy and adhesion properties, but there are competing reactions between the plasma species generated from O_2 and CF_4.[37] While oxygen species are used to make surfaces more wetting, atomic fluorine and molecules consisting of fluorine may act as etchants or can react with the substrate to make surfaces hydrophobic, nonwetting to polar solvents, and nonsticking. The ratio of O_2/CF_4 gases in the plasma will greatly affect the surface modification imparted to the substrate.[38] In fact, in gas ratios as low as 40:60 (O_2/CF_4), oxidation of the substrate is preferentially accelerated, thus creating a more hydrophilic surface.[39] Since the gas ratio used in these treatments was 1:1:98 (O_2/CF_4/He), the MWCNT arrays were oxidized and made fully wetting.

Pristine and functionalized MWCNT arrays were characterized with Raman spectroscopy to elucidate changes in the MWCNT structure and defect density. In sp^2-bonded carbon materials, it is common to compare the ratio of intensities of the G-band (~1580 cm^{-1}), which arises from in-plane vibrations of graphite and the material disorder induced D-band (~1350 cm^{-1}). Predominance of the G-band over the D-band corresponds to a highly graphitic sample with a relatively small presence of disorder due to chemical impurities, structural defects, or amorphous material. Representative spectra for all samples are plotted in Figure 3. Though all arrays had predominantly higher G-bands, they exhibited varying degrees of defect density based on surface treatment. Pristine arrays had an average G/D ratio of 2.06, which confirms that the as-grown samples have a low defect density. The ratio nearly doubled after graphitization, with an average of 3.78 attributed to healing of defects. Additionally, the D-band peak width decreases, which signifies the removal of amorphous carbon. PyC deposition results in a decrease of the average G/D ratio to 1.7 and a broadening of the D-bandwidth, resulting from coating the MWCNTs with disordered sp^3-rich carbonaceous material. After O_2/CF_4 plasma functionalization, all G/D ratios are observed to decrease due to incurred defects in the form of broken and dangling bonds plus incorporation of oxygen-containing functional groups.

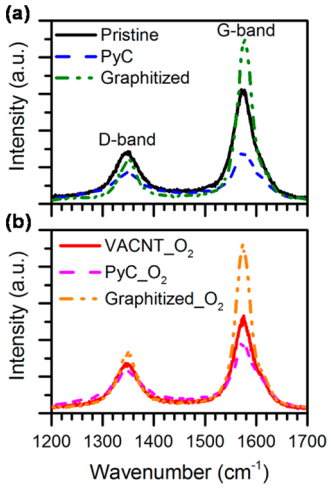

Figure 3. Raman spectra were collected from post-treated VACNT arrays with (b) and without (a) plasma functionalization treatments to characterize changes in defect density.

Prior research has shown that after an ALD coating, the G/D ratio and peak intensities will decrease due to the inability of coated CNTs to resonate at the same magnitude as uncoated CNTs.[3,23] This was generally true for these samples with the exception of G_100, O_2_100, and G + O_2_100 arrays. For these samples, the G/D ratio increased after ALD coating, especially for the latter. Though the exact reason for this behavior is unclear, we suspect that the increasing G/D ratio is the result of a shielding effect caused by preferential grafting of nucleated alumina to functional defect sites on the MWCNT surfaces. This effect has been previously observed in the grafting of metal nanoparticles to CNT surfaces.[40]

3.2. Al_2O_3 Distribution in VACNT Arrays. Cross-sectional SEM analysis of sections located in the center of the ALD coated arrays, shown in Figure 4a, reveal an uneven distribution of Al_2O_3 through the array thickness. A visible gradient from top to bottom caused by charging induced bright field contrast indicates an accumulation of insulating Al_2O_3 material. This effect was especially apparent in the cross-section of samples which were plasma treated prior to ALD, which are presented in Figures S6–S8. The uneven distribution was further confirmed using EDS spectral analysis acquired at the top, middle, and bottom of each ALD coated array, and the change in Al concentration was quantified using an Al_2O_3 standard. All samples were observed to have a higher concentration of Al at the top of the array. This disparity was maximized for plasma treated samples, the highest top surface concentration being 34.4 atom %, followed by 28.6 atom % and 28 atom % for O_2_100, G+O_2_100, and PyC+O_2_100, respectively. Plasma

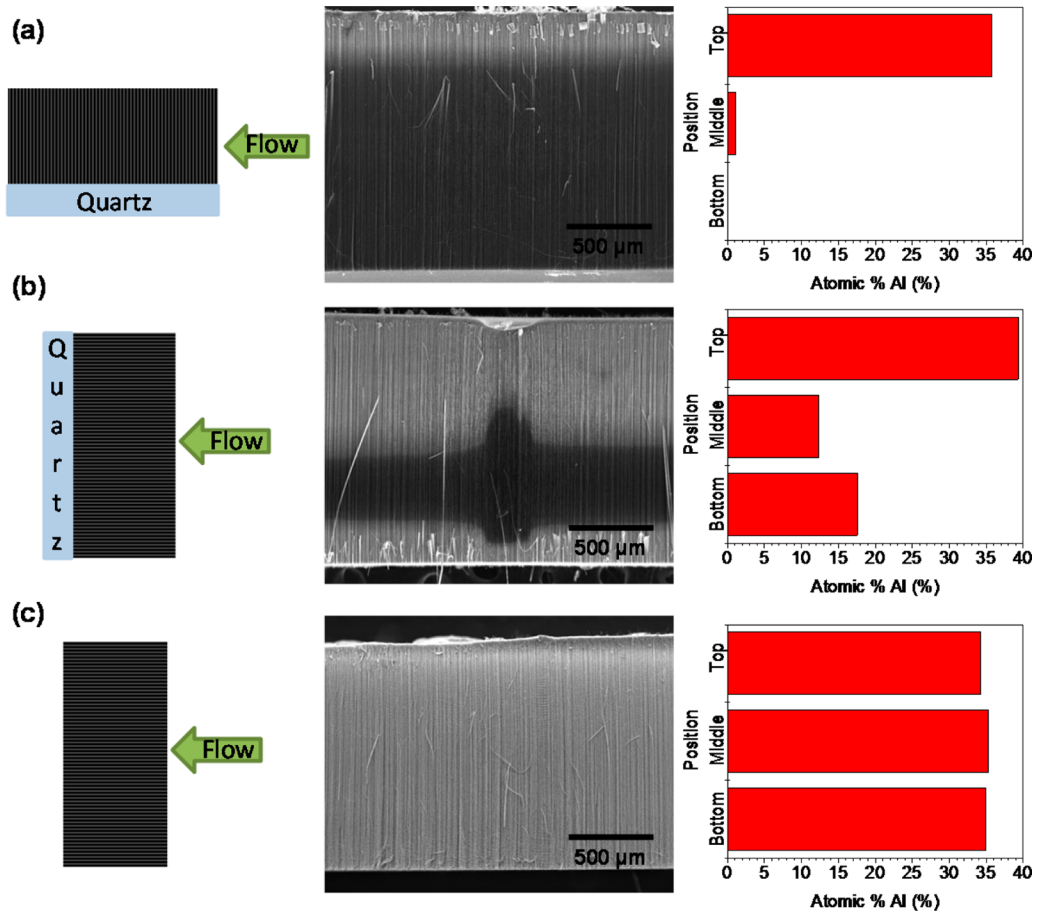

Figure 4. EDS analysis at the top, middle, and bottom of each ALD coated array. The atomic % of Al was measured through the thickness as a function of experimental setup. (a) The MWCNT axes were aligned perpendicular to the flow of ALD precursor, and the array remained on the quartz growth substrate. This resulted in a high concentration of Al at the top of the array, which rapidly decreased through the thickness. (b) The array mounted to the quartz was then rotated 90° so that the MWCNT axes were oriented parallel to precursor flow. (c) Finally, Al was homogeneously dispersed throughout the MWCNT array, which was both removed from the quartz growth substrate and rotated.

treatment can preferentially functionalize the top of VACNT arrays due to increased bombardment by energetic species. Furthermore, as these arrays are known to grow via base growth, the MWCNT tips are likely to have many defects. These defects would have an affinity for oxidation during plasma treatment in the O_2 atmosphere.

Generally, the Al concentration decreases through the thickness of the array. As shown in Figure S8, this effect was somewhat mitigated for graphitized samples which had higher Al concentrations at the top and bottom of the array, with a depleted region in the middle. Prior to high temperature heat treatment, these VACNTs were removed from the quartz growth substrate to prevent melting. By removing the quartz, ALD precursors were able to diffuse into the array from the top and bottom, creating the unique concentration profile.

A similar concentration profile was found to occur when arrays still mounted to the quartz were turned 90° so that the MWCNT axes were parallel to the precursor flow, as can be seen in Figure 4b. It is suspected that the quartz substrate causes a gas turbulence within the array and extending outward from the sample surface. This turbulence prevents satisfactory purging and delivery of reactants to the VACNT array. As a result, CVD-like growth occurred at the array surface, further inhibiting adequate product removal and prohibiting ideal ALD nucleation and growth throughout the sample cross-section. In previous studies of ALD on high aspect ratio materials, this nonideal behavior has been attributed to site blocking by reaction byproducts.[41] Only by both rotating the array as well as removing it from the quartz substrate could a uniform Al distribution be achieved, as shown in Figure 4c. A sample holder was fabricated to carefully sandwich the array between two pieces of PET mesh screen and suspend it in the middle of the ALD reactor cross-section. This technique was used to produce all arrays for mechanical testing and thermal analysis. These samples included pristine and PyC+O_2 arrays coated for 100 cycles (VACNT_100 and PyC+O_2_100, respectively) as well as PyC+O_2 coated for 500 cycles (PyC+O_2_500). SEM micrographs showing the thick conformal coatings for samples coated for 500 cycles are shown in Figure 5.

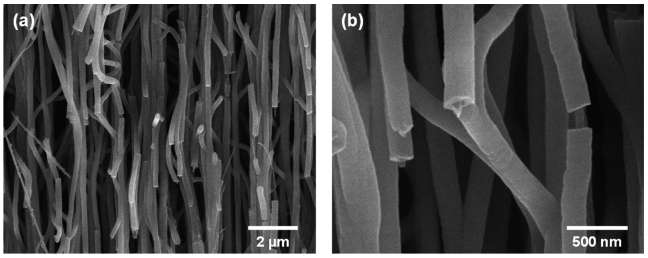

Figure 5. SEM micrographs of pretreated VACNT arrays after 500 cycles of Al_2O_3 ALD at (a) low and (b) high magnification. Both images were taken from the middle section of the coated array.

It is generally accepted that the aligned nature of VACNT arrays is beneficial in promoting ideal ALD-type growth compared to more dense, randomly oriented CNT structures such as buckypapers.[42] Aligned structures have more free space between adjacent CNTs, which allows for easier precursor diffusion and purging. This alone, however, does not guarantee uniform coating thickness through the array cross-section. Nonuniform coating thickness as a function of precursor penetration depth has been demonstrated by other researchers working with VACNT arrays.[7,10] It has been theoretically and experimentally determined that this is caused by the decreasing pore diameter with additional ALD cycles which hinders the diffusion of precursor molecules.[28,43] Additionally, with more ALD cycles, the surface area of the VACNT array increases, meaning more precursor molecules and/or longer exposures are required with each subsequent cycle to satisfy all available active sites on the CNT surfaces. In the case of ALD on anodic alumina, another high aspect ratio structure, large precursor dose (120 s) and purging times (240 s) were required to uniformly coat the anodic alumina membrane through the whole thickness.[26] None of these prior studies investigated the effect of rotating the long pore axis parallel to the direction of precursor flow. Though longer purge times were used in this current study (30 and 45 s for TMA and H_2O, respectively), a uniform coating thickness was achieved without increasing the overall exposure despite the ever-decreasing pore diameter.

TGA and dTGA curves for coated and uncoated arrays, with and without surface treatments, are shown in Figure 6. The

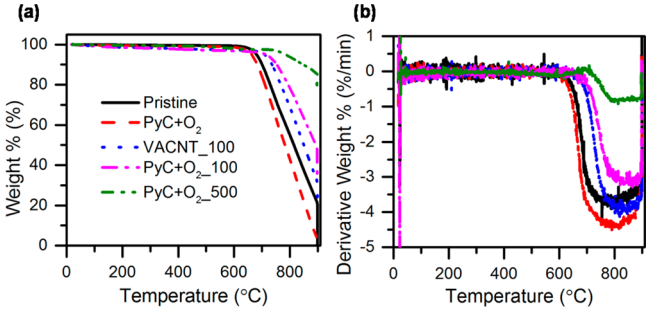

Figure 6. (a) TGA and (b) dTGA plots show improvement in oxidation resistance of all alumina ALD coated CNT samples compared to as-grown.

large drop in mass above 600 °C corresponds to the decomposition of the MWCNTs due to thermal oxidation. The onset of this decomposition (T_{onset}) is shifted toward higher temperatures for all ALD coated samples, though by varying amounts. Without any surface pretreatment, T_{onset} increased significantly from 670 to 730 °C following 100 cycles of Al_2O_3 ALD. Additionally, the mass remaining following a 30 min isothermal soak at 900 °C increased from 0.52 wt % to 24.1 wt % after ALD treatment, corresponding to the weight of deposited alumina. The addition of PyC deposition and plasma treatment did not significantly change the thermal behavior of pristine arrays, but after 100 ALD cycles, the T_{onset} increased to 744 °C with almost 36 wt % remaining. The higher onset and increased mass remaining are a result of more uniform nucleation and coating on the MWCNT array. The greatest improvement in thermal stability was measured for surface pretreated samples coated with 500 cycles of Al_2O_3, with T_{onset} = 763 °C. The decomposition rate was significantly lower than others tested, only 0.9%/min as a result of the thick Al_2O_3 coatings that uniformly coat and protect the MWCNTs from oxidation. Interestingly a small increase in mass was repeatedly observed around 500 °C for samples coated with 500 cycles of Al_2O_3. We suspect that this is a result of the incorporation of oxygen from the atmosphere into the amorphous Al_2O_3 as it is heated. Aksel and Eder investigated the oxidation resistance of many metal oxide−CNT hybrids, including Al_2O_3, fabricated via a modified sol−gel technique.[44] They found that Al_2O_3−CNT hybrids

exhibited improved resistance to thermal oxidation by almost 100 °C, which agrees well with our results.

All samples were fully calcined after TGA testing, leaving behind arrays of vertically aligned Al_2O_3 nanotubes, which are shown in Figure 7. The Al_2O_3 arrays were found to be

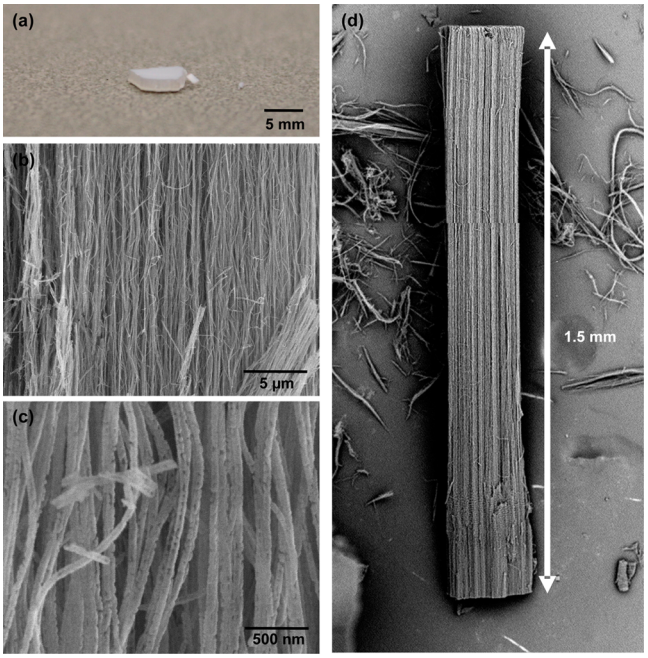

Figure 7. VACNTs removed via oxidation to leave behind a vertically aligned network of alumina nanotubes with high porosity and high surface area.

continuous through the thickness with high porosity and surface area. The porosity is likely a product of CO_2 gas release upon thermal oxidation of the MWCNT walls. Al_2O_3 nanotubes have previously been produced by coating CNTs using solution methods followed by CNT removal via oxidation, and though the resulting structure had a high surface area (60 m^2 g^{-1}) it was also discontinuous and highly fragmented.[45] The creation of aligned Al_2O_3 nanotubes using the ALD technique is straightforward and can be easily controlled by varying the height of the MWCNT array and the thickness of the ALD coating.

Compression testing was carried out on pristine and functionalized VACNT arrays to compare the mechanical responses of the arrays with and without ALD coatings. Due to their ultralow density, as-grown VACNT arrays have poor mechanical properties, as can be seen from the stress−strain plots in Figure 8. The modulus is observed to increase from 0.83 MPa for the pristine arrays to 3.24 MPa simply after ALD coating. Even more significant is the increase in the compressive modulus of functionalized arrays after ALD coating (PyC+O_2_100), which nearly triples to 11.11 MPa. This large increase is attributed to the uniform coating of the VACNTs throughout the entire array rather than sparse nucleation that was found to occur on pristine, non-functionalized VACNTs. In the case of the latter, nucleated Al_2O_3 beads on the MWCNT surface do not participate in load transfer in the same manner than a concentric, conformal Al_2O_3 coating would. Another explanation could also be that the strong presence of functional groups on the MWCNT surfaces can improve interfacial bonding between the MWCNT surface

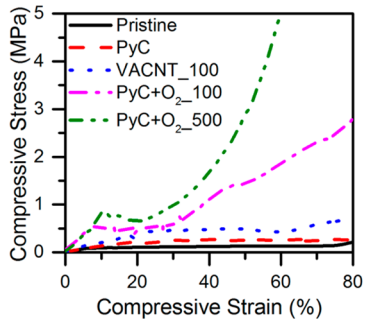

Figure 8. Compressive stress−strain curves for ALD coated and uncoated VACNTs. Arrays which underwent surface activation prior to ALD coating (PyC+O_2_100 and PyC+O_2_500) exhibited a larger enhancement in compressive properties compared to uncoated and nonfunctionalized arrays (Pristine, PyC, VACNT_100).

and Al_2O_3 film. It is also interesting to note that these particular samples exhibited foam-like recovery of nearly 100% after the compressive load was removed. In earlier work, this researcher and others have fabricated VACNT sponges via PyC deposition.[33,46] It is impressive that the foam properties can be maintained and even enhanced with the addition of a 12 nm thick alumina coating. The modulus was further improved to 12.81 MPa by coating the functionalized arrays for 500 cycles. The compressive strengths at 20% and 60% strain for each array was also measured. At low strains, the compressive strength is also low due to buckling of the VACNT forest structure. An increase was observed for higher strains, however, as the samples were densified and consolidated during compression. At 60% strain, the compressive strength increased from 0.15 to 2.16 MPa after only adding 100 cycles of alumina ALD. After 500 cycles, the compressive strength further increased to 6.32 MPa. These values are especially impressive when one considers the low density of even the ALD coated VACNT arrays. The average compressive moduli and strength values are summarized in Table 1.

Table 1. Average Compressive Modulus and Strength Values for ALD Coated and Uncoated VACNTs

sample	modulus (MPa)	strength @ 20% (MPa)	strength @ 60% (MPa)
pristine	0.83 ± 0.16	0.11 ± 0.002	0.15 ± 0.01
PyC	1.34 ± 0.29	0.24 ± 0.05	0.37 ± 0.11
VACNT_100	3.24 ± 0.60	0.44 ± 0.07	0.56 ± 0.10
PyC_O_2_100	11.11 ± 3.42	0.61 ± 0.10	2.16 ± 0.18
Pyc_O_2_500	12.81 ± 3.27	0.71 ± 0.22	6.32 ± 0.96

An additional benefit to coating the MWCNT arrays with Al_2O_3 is their improved ability to be processed into ceramic composites. One common route for the manufacture of toughened ceramic composites is the addition of CNTs to ceramic powders prior to consolidating and sintering.[47] There are several issues with this method however. First, CNTs are prone to agglomeration due to mutual van der Waals attractions. Second, due to large differences in density between the ceramic powders and CNTs, it is difficult to achieve a uniform dispersion of CNTs in the matrix, which results in a worsening in properties. Additionally, because pristine CNTs are for the majority inert, they will exhibit little to no interfacial bonding with the surrounding matrix. Finally, due to the presence of oxygen during many sintering techniques, CNTs

are prone to degradation from thermal oxidation. The ALD Al_2O_3 coated MWCNTs fabricated in this study have the potential to resolve these issues due to the observed improvements in thermal stability and mechanical robustness. In addition, the coated MWCNT surfaces are effectively surface functionalized by their being conformally coated in oxygen-rich Al_2O_3. As shown in Figure 9, arrays coated for 100 cycles are

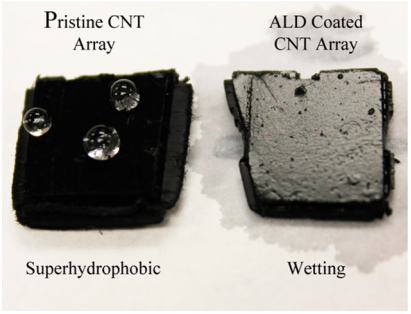

Figure 9. Pristine VACNT arrays. These are superhydrophobic due to high surface roughness and low CNT density in the array. After 100 cycles of Al_2O_3 ALD, the surface energy of the coating dominates over the physical structure and the arrays wet.

easily wettable by water and other aqueous solutions where pristine arrays are typically hydrophobic due to high hierarchical micro- and nanoscale surface roughness.

4. CONCLUSIONS

ALD is a useful technique for the uniform and conformal coating of high surface area and high aspect ratio VACNT arrays, but not without first optimizing the sample and process parameters for best results. The surface chemistry of high graphitic quality, low defect density MWCNTs was optimized for Al_2O_3 nucleation via PyC deposition and oxygen plasma functionalization. The combination of these two surface pretreatments provided a high concentration of oxygen-containing functional groups that could complex with TMA upon dosing, thus creating a high nucleation density of Al_2O_3 on the MWCNT surface, which then quickly spread and coalesced into a thin film. Furthermore, a uniform distribution of Al_2O_3 through the thickness of the array was achieved by removing the MWCNTs from their growth substrate and orienting the MWCNT axes parallel to the flow of the reactor. It was determined that the Al_2O_3 coated MWCNTs not only exhibited greatly enhanced compressive properties, but also improved thermal stability to oxidation by delaying onset by nearly 100 °C. To the best of the authors' knowledge, this is the first demonstration of conformal ALD coating of 1.5 mm long VACNTs with a pore aspect ratio ~15 000.

■ ASSOCIATED CONTENT

Supporting Information

(Figure S1) Experimental apparatus used to mount MWCNT array with CNT axes parallel to precursor flow in ALD chamber. (Figure S2) SEM images of as-grown VACNT array cross-section. Inset shows TEM image of typical MWNT used in experiments. (Figure S3) EDS spectrum from an as-grown array. (Figure S4) TEM images of alumina nucleation on as grown MWCNTs. (Figure S5) TEM images after 100 cycles of alumina ALD on graphitized and PyC coated MWCNTs. (Figure S6) TEM images after 100 cycles of alumina ALD on all oxygen plasma functionalized MWCNT samples. (Figures S7–S9) Cross-sectional SEM and accompanying EDS measurements taken from top to bottom through the ALD-coated arrays. This material is available free of charge via the Internet at http://pubs.acs.org.

■ AUTHOR INFORMATION

Corresponding Author

*Tel.: +1-919-515-1866. Fax: +1-919-515-6532. E-mail: philip_bradford@ncsu.edu.

Notes

The authors declare no competing financial interest.

■ ACKNOWLEDGMENTS

The authors acknowledge the use of the Analytical Instrumentation Facility (AIF) at North Carolina State University, which is supported by the State of North Carolina and the National Science Foundation. This material is based upon work supported by the National Science Foundation Graduate Research Fellowship Program under grant no. DGE-0946818. The authors thank Prof. Yuntian Zhu for time on the Raman Microscope.

■ REFERENCES

(1) Eder, D. Carbon Nanotube-Inorganic Hybrids. *Chem. Rev.* **2010**, *110*, 1348–1385.

(2) Lee, J. S.; Min, B.; Cho, K.; Kim, S.; Park, J.; Lee, Y. T.; Kim, N. S.; Lee, M. S.; Park, S. O.; Moon, J. T. Al_2O_3 Nanotubes and Nanorods Fabricated by Coating and Filling of Carbon Nanotubes with Atomic-Layer Deposition. *J. Cryst. Growth* **2003**, *254*, 443–448.

(3) Liyanage, L. S.; Cott, D. J.; Delabie, A.; Van Elshocht, S.; Bao, Z.; Wong, H.-S. P. Atomic Layer Deposition of High-K Dielectrics on Single-Walled Carbon Nanotubes: A Raman Study. *Nanotechnology* **2013**, *24*, 245703.

(4) Javey, A.; Kim, H.; Brink, M.; Wang, Q.; Ural, A.; Guo, J.; McIntyre, P.; McEuen, P.; Lundstrom, M.; Dai, H. High-K Dielectrics for Advanced Carbon-Nanotube Transistors and Logic Gates. *Nat. Mater.* **2002**, *1*, 241–246.

(5) Gomathi, A.; Vivekchand, S. R. C.; Govindaraj, A.; Rao, C. N. R. Chemically Bonded Ceramic Oxide Coatings on Carbon Nanotubes and Inorganic Nanowires. *Adv. Mater.* **2005**, *17*, 2757–2761.

(6) Kim, D. S.; Lee, S.-M.; Scholz, R.; Knez, M.; Gösele, U.; Fallert, J.; Kalt, H.; Zacharias, M. Synthesis and Optical Properties of ZnO and Carbon Nanotube Based Coaxial Heterostructures. *Appl. Phys. Lett.* **2008**, *93*, 103108.

(7) Hu, C. J.; Lin, Y. H.; Tang, C. W.; Tsai, M. Y.; Hsu, W. K.; Kuo, H. F. ZnO-Coated Carbon Nanotubes: Flexible Piezoelectric Generators. *Adv. Mater.* **2011**, *23*, 2941–2945.

(8) Boukhalfa, S.; Evanoff, K.; Yushin, G. Atomic Layer Deposition of Vanadium Oxide on Carbon Nanotubes for High-Power Supercapacitor Electrodes. *Energy Environ. Sci.* **2012**, *5*, 6872.

(9) Hsueh, Y.-C.; Wang, C.-C.; Liu, C.; Kei, C.-C.; Perng, T.-P. Deposition of Platinum on Oxygen Plasma Treated Carbon Nanotubes by Atomic Layer Deposition. *Nanotechnology* **2012**, *23*, 405603.

(10) Dameron, A. A.; Pylypenko, S.; Bult, J. B.; Neyerlin, K. C.; Engtrakul, C.; Bochert, C.; Leong, G. J.; Frisco, S. L.; Simpson, L.; Dinh, H. N.; et al. Aligned Carbon Nanotube Array Functionalization for Enhanced Atomic Layer Deposition of Platinum Electrocatalysts. *Appl. Surf. Sci.* **2012**, *258*, 5212–5221.

(11) Min, Y.-S.; Bae, E. J.; Jeong, K. S.; Cho, Y. J.; Lee, J.-H.; Choi, W. B.; Park, G.-S. Ruthenium Oxide Nanotube Arrays Fabricated by Atomic Layer Deposition Using a Carbon Nanotube Template. *Adv. Mater.* **2003**, *15*, 1019–1022.

(12) Herrmann, C. F.; Fabreguette, F. H.; Finch, D. S.; Geiss, R.; George, S. M. Multilayer and Functional Coatings on Carbon

Nanotubes Using Atomic Layer Deposition. *Appl. Phys. Lett.* **2005**, *87*, 123110.
(13) Lahiri, I.; Oh, S.-M.; Hwang, J. Y.; Kang, C.; Choi, M.; Jeon, H.; Banerjee, R.; Sun, Y.-K.; Choi, W. Ultrathin Alumina-Coated Carbon Nanotubes as an Anode for High Capacity Li-Ion Batteries. *J. Mater. Chem.* **2011**, *21*, 13621.
(14) Fu, L.; Liu, Y. Q.; Liu, Z. M.; Han, B. X.; Cao, L. C.; Wei, D. C.; Yu, G.; Zhu, D. B. Carbon Nanotubes Coated with Alumina as Gate Dielectrics of Field-Effect Transistors. *Adv. Mater.* **2006**, *18*, 181−185.
(15) Dillon, A. C.; Ott, A. W.; Way, J. D.; George, S. M. Surface Chemistry of Al_2O_3 Deposition Using $Al(CH_3)_3$ and H_2O in a Binary Reaction Sequence. *Surf. Sci.* **1995**, *322*, 230−242.
(16) Ott, A. W.; Klaus, J. W.; Johnson, J. M.; George, S. M. Al_3O_3 Thin Film Growth on Si(100) Using Binary Reaction Sequence Chemistry. *Thin Solid Films* **1997**, *292*, 135−144.
(17) Groner, M. D.; Fabreguette, F. H.; Elam, J. W.; George, S. M. Low-Temperature Al_2O_3 Atomic Layer Deposition. *Chem. Mater.* **2004**, 639−645.
(18) Puurunen, R. L. Surface Chemistry of Atomic Layer Deposition: A Case Study for the Trimethylaluminum/water Process. *J. Appl. Phys.* **2005**, *97*, 121301.
(19) Farmer, D. B.; Gordon, R. G. ALD of High-K Dielectrics on Suspended Functionalized SWNTs. *Electrochem. Solid-State Lett.* **2005**, *8*, G89.
(20) Zhan, G.-D.; Du, X.; King, D. M.; Hakim, L. F.; Liang, X.; McCormick, J. A.; Weimer, A. W. Atomic Layer Deposition on Bulk Quantities of Surfactant-Modified Single-Walled Carbon Nanotubes. *J. Am. Ceram. Soc.* **2008**, *91*, 831−835.
(21) Min, Y.-S.; Lee, I. H.; Lee, Y. H.; Hwang, C. S. Botryoidal Growth of Crystalline ZnO Nanoparticles on a Forest of Single-Walled Carbon Nanotubes by Atomic Layer Deposition. *CrystEngComm* **2011**, *13*, 3451.
(22) Marichy, C.; Tessonnier, J.-P.; Ferro, M. C.; Lee, K.-H.; Schlögl, R.; Pinna, N.; Willinger, M.-G. Labeling and Monitoring the Distribution of Anchoring Sites on Functionalized CNTs by Atomic Layer Deposition. *J. Mater. Chem.* **2012**, *22*, 7323.
(23) Devine, C. K.; Oldham, C. J.; Jur, J. S.; Gong, B.; Parsons, G. N. Fiber Containment for Improved Laboratory Handling and Uniform Nanocoating of Milligram Quantities of Carbon Nanotubes by Atomic Layer Deposition. *Langmuir* **2011**, *27*, 14497−14507.
(24) Farmer, D. B.; Gordon, R. G. Atomic Layer Deposition on Suspended Single-Walled Carbon Nanotubes via Gas-Phase Noncovalent Functionalization. *Nano Lett.* **2006**, *6*, 699−703.
(25) Cavanagh, A. S.; Wilson, C. A.; Weimer, A. W.; George, S. M. Atomic Layer Deposition on Gram Quantities of Multi-Walled Carbon Nanotubes. *Nanotechnology* **2009**, *20*, 255602.
(26) Elam, J.; Routkevitch, D.; Mardilovich, P. P.; George, S. M. Conformal Coating on Ultrahigh-Aspect-Ratio Nanopores of Anodic Alumina by Atomic Layer Deposition. *Chem. Mater.* **2003**, 3507−3517.
(27) Elam, J. W.; Libera, J. A.; Huynh, T. H.; Feng, H.; Pellin, M. J. Atomic Layer Deposition of Aluminum Oxide in Mesoporous Silica Gel. *J. Phys. Chem. C* **2010**, *114*, 17286−17292.
(28) Yazdani, N.; Chawla, V.; Edwards, E.; Wood, V.; Park, H. G.; Utke, I. Modeling and Optimization of Atomic Layer Deposition Processes on Vertically Aligned Carbon Nanotubes. *Beilstein J. Nanotechnol.* **2014**, *5*, 234−244.
(29) Inoue, Y.; Kakihata, K.; Hirono, Y.; Horie, T.; Ishida, A.; Mimura, H. One-Step Grown Aligned Bulk Carbon Nanotubes by Chloride Mediated Chemical Vapor Deposition. *Appl. Phys. Lett.* **2008**, *92*, 213113.
(30) Puurunen, R. L.; Vandervorst, W.; Besling, W. F. A.; Richard, O.; Bender, H.; Conard, T.; Zhao, C.; Delabie, A.; Caymax, M.; De Gendt, S.; et al. Island Growth in the Atomic Layer Deposition of Zirconium Oxide and Aluminum Oxide on Hydrogen-Terminated Silicon: Growth Mode Modeling and Transmission Electron Microscopy. *J. Appl. Phys.* **2004**, *96*, 4878.
(31) Andrews, R.; Jacques, D.; Qian, D.; Dickey, E. C. Purification and Structural Annealing of Multiwalled Carbon Nanotubes at Graphitization Temperatures. *Carbon* **2001**, *39*, 1681−1687.
(32) Faraji, S.; Stano, K.; Rost, C.; Maria, J.-P.; Zhu, Y.; Bradford, P. D. Structural Annealing of Carbon Coated Aligned Multi-Walled Carbon Nanotube Sheets. *Carbon* **2014**, 1−10.
(33) Bradford, P. D.; Wang, X.; Zhao, H.; Zhu, Y. T. Tuning the Compressive Mechanical Properties of Carbon Nanotube Foam. *Carbon* **2011**, *49*, 2834−2841.
(34) Zheng, G.-B.; Sano, H.; Uchiyama, Y. A Layer-by-Layer Deposition Mechanism for Producing a Pyrolytic Carbon Coating on Carbon Nanotubes. *Carbon* **2013**, *57*, 267−273.
(35) Jensen, D. S.; Kanyal, S. S.; Gupta, V.; Vail, M. A.; Dadson, A. E.; Engelhard, M.; Vanfleet, R.; Davis, R. C.; Linford, M. R. Stable, Microfabricated Thin Layer Chromatography Plates without Volume Distortion on Patterned, Carbon and Al_2O_3-Primed Carbon Nanotube Forests. *J. Chromatogr. A* **2012**, *1257*, 195−203.
(36) Hontoria-Lucas, C.; López-Peinado, A. J.; López-González, J.; de, D.; Rojas-Cervantes, M. L.; Martín-Aranda, R. M. Study of Oxygen-Containing Groups in a Series of Graphite Oxides: Physical and Chemical Characterization. *Carbon* **1995**, *33*, 1585−1592.
(37) Kanazawa, S.; Kogoma, M.; Okazaki, S.; Moriwaki, T. Glow Plasma Treatment at Atmospheric Pressure for Surface Modification and Film Deposition. *Nucl. Instrum. Methods Phys. Res.* **1989**, *38*, 842−845.
(38) Kogoma, M.; Kasai, H.; Takahashi, K.; Moriwaki, T.; Okazaki, S. Wettability Control of a Plastic Surface by CF_4-O_2 Plasma and Its Etching Effect. *J. Phys. D. Appl. Phys.* **1987**, *20*, 147−149.
(39) Occhiello, E.; Morra, M.; Gardassi, F.; Bargon, J. On the Application of XPS, SSIMS and QCM to Study the Surface of a CF_4/O_2 Plasma Treated Polycarbonate. *Appl. Surf. Sci.* **1989**, *36*, 285−295.
(40) Mohan, R.; Shanmugharaj, A. M.; Sung, R. H. An Efficient Growth of Silver and Copper Nanoparticles on Multiwalled Carbon Nanotube with Enhanced Antimicrobial Activity. *J. Biomed. Mater. Res., Part B* **2011**, *96B*, 119−126.
(41) Kucheyev, S. O.; Biener, J.; Baumann, T. F.; Wang, Y. M.; Hamza, A. V.; Li, Z.; Lee, D. K.; Gordon, R. G. Mechanisms of Atomic Layer Deposition on Substrates with Ultrahigh Aspect Ratios. *Langmuir* **2008**, *24*, 943−948.
(42) Li, X. L.; Li, C.; Zhang, Y.; Chu, D. P.; Milne, W. I.; Fan, H. J. Atomic Layer Deposition of ZnO on Multi-Walled Carbon Nanotubes and Its Use for Synthesis of CNT-ZnO Heterostructures. *Nanoscale Res. Lett.* **2010**, *5*, 1836−1840.
(43) George, S. M. Atomic Layer Deposition: An Overview. *Chem. Rev.* **2010**, *110*, 111−131.
(44) Aksel, S.; Eder, D. Catalytic Effect of Metal Oxides on the Oxidation Resistance in Carbon Nanotube−Inorganic Hybrids. *J. Mater. Chem.* **2010**, *20*, 9149.
(45) Satishkumar, B. C.; Govindaraj, A.; Vogl, E. M.; Basumallick, L.; Rao, C. N. R. Oxide Nanotubes Prepared Using Carbon Nanotubes as Templates. *J. Mater. Res.* **2011**, *12*, 604−606.
(46) Stano, K. L.; Chapla, R.; Carroll, M.; Nowak, J.; McCord, M.; Bradford, P. D. Copper Encapsulated Vertically Aligned Carbon Nanotube Arrays. *ACS Appl. Mater. Interfaces* **2013**, *5*, 10774−10781.
(47) Cho, J.; Boccaccini, A. R.; Shaffer, M. S. P. Ceramic Matrix Composites Containing Carbon Nanotubes. *J. Mater. Sci.* **2009**, *44*, 1934−1951.